metals

Article

Energy–Quality Balanced Optimization in Multi-Roll Leveling Parameters for Ultra-High-Strength Steel Considering Initial Wave Heights

Xuhui Xia [1,2], Baorong Fu [1,2], Zelin Zhang [1,2,*], Lei Wang [1,2], Yuyao Guo [1,2] and Jianhua Cao [1,2]

[1] Key Laboratory of Metallurgical Equipment and Control Technology, Ministry of Education, Wuhan University of Science and Technology, Wuhan 430081, China; xiaxuhui@wust.edu.cn (X.X.); fbr1982@163.com (B.F.); candywang@wust.edu.cn (L.W.); guoyuyao@wust.edu.cn (Y.G.); caojianhua39@wust.edu.cn (J.C.)
[2] Hubei Key Laboratory of Mechanical Transmission and Manufacturing Engineering, Wuhan University of Science and Technology, Wuhan 430081, China
* Correspondence: zhangzelin@wust.edu.cn

Abstract

In the leveling process of ultra-high-strength steel plates, sample scarcity—driven by high prototyping costs and small-batch production—coupled with a narrow and unevenly distributed feasible region due to high yield-to-tensile ratios and limited ductility, impedes the balanced optimization of plate shape quality and energy consumption. To address this issue, this paper develops an optimization framework for the balanced trade-off between these two objectives. First, a high-precision response surface model based on Box–Behnken experimental design and finite element simulation was constructed using initial wave height, entry roll reduction, exit roll reduction, and leveling speed as key process parameters; peak residual stress difference (characterizing potential sheet quality) and leveling energy consumption as co-optimization objectives; and post-leveling flatness as a constraint. Next, by introducing the NSGA-II multi-objective genetic algorithm, the Pareto optimal solution set for the quality and energy efficiency objectives was obtained, clearly revealing the trade-off relationship between the two; furthermore, the TOPSIS decision-making method was employed to select the comprehensive optimal process scheme that achieves a balance between quality and energy efficiency from the Pareto solution set. An adaptive recommendation curve for the leveling process parameters of MS1500 ultra-high-strength steel plates was established, covering an initial wave height range of 10.5–14.6 mm, thereby enabling intelligent parameter matching based on different incoming material conditions. Finally, industrial validation demonstrated that this optimized scheme significantly reduced leveling energy consumption while ensuring that post-leveling flatness meets the high-quality requirement of less than 3.5 mm·m^{-1}. This achieves a balanced optimization of quality and energy efficiency. This study provides a reliable theoretical basis and practical engineering solution for the efficient and environmentally friendly leveling production of ultra-high-strength steel.

Keywords: energy–quality balanced optimization; multi-roll leveling; ultra-high-strength steel; post-leveling flatness; total leveling force; leveling energy consumption; response surface methodology; NSGA-II

Check for updates

Academic Editor: Zbigniew Pater

Received: 5 June 2026
Revised: 7 July 2026
Accepted: 7 July 2026
Published: 9 July 2026

Copyright: © 2026 by the authors. Licensee MDPI, Basel, Switzerland. This article is an open access article distributed under the terms and conditions of the Creative Commons Attribution (CC BY) license.

1. Introduction

Ultra-high-strength steel plates possess excellent specific strength, toughness, and fatigue resistance, making them strategic materials for critical sectors such as heavy machinery, aerospace, marine engineering, and defense equipment [1,2]. As the final shape-control process before sheet and strip products leave the mill, the operators' level of experience of multi-roll leveling directly determines the flatness and internal residual stress state of the product [3], exerting a decisive influence on the precision and efficiency of downstream manufacturing processes. Compared to steel of conventional strength grades, the high-strength, low-ductility, and high-springback characteristics of ultra-high-strength steel fundamentally alter the mechanical response and energy distribution during the leveling process. To achieve good post-leveling flatness and improve residual stress (i.e., leveling quality), it is often necessary to apply greater leveling forces and employ more complex bending paths, leading to a significant increase in equipment energy consumption and highlighting the "energy–quality" trade-off. Therefore, developing an energy–quality co-optimization method that effectively controls energy consumption while ensuring leveling quality is an effective approach to driving the intelligent and green transformation of the metallurgical equipment industry.

However, the energy–quality co-optimization of ultra-high-strength steel leveling is not a simple extension of the multi-objective optimization problems associated with steel of conventional strength grades. The reason for this is twofold: on the one hand, the production characteristics of ultra-high-strength steel—involving multiple grades and small batches—result in a scarcity of process data, making it difficult to conduct intelligent optimization of process parameters using big data fitting or predictive models, as is done with steel of conventional strength grades. On the other hand, the constitutive properties of UHSS make it more prone to significant residual stress gradients and cross-sectional stress asymmetry during the leveling process [4], resulting in structural distortions in the feasible space for process parameter optimization: first, the sensitivity of sheet quality metrics (such as post-leveling flatness and residual stress) to process parameters exhibits a steep nonlinear increase, drastically compressing the global feasible space that satisfies all constraints and resulting in a typical "narrow window" characteristic; second, the optimization of any single objective (sheet flatness, leveling energy consumption) tends to cause a sharp deterioration in the other objective, resulting in a discontinuous distribution of feasible solutions in the parameter space.

Numerous scholars have conducted extensive research on the modeling and optimization of leveling processes. Early studies primarily focused on mild steel, aiming to elucidate the mechanisms by which key process parameters, such as reduction ratio, affect leveling quality through experimental research, analytical methods, and numerical simulations. In terms of experimental research, Japanese scholars [5] developed a model for the leveling of sheet metal subjected to repeated bending deformation through experiments and preliminarily revealed the quantitative relationship between the entry reduction and residual curvature.

In terms of analytical methods, Doege et al. [6] developed analytical models for calculating residual stress, residual curvature, and leveling force based on linearly hardening materials, specifically addressing the multi-pass bending deformation of sheet metal during the leveling process. Wang et al. [7] derived the working roll reduction for a seven-roll straightener under a large deformation scheme, reproduced the deformation trajectory of the strip corresponding to this reduction schedule, and calculated the leveling quality based on the trajectory curve. Regarding the multi-roll leveling process for medium- and heavy-gauge plates, Liu [8] investigated the evolution laws of key process parameters and force–energy parameters during the adjustment of the reduction ratio, starting

from the derivation of models for leveling force and torque. Kuo et al. [9] constructed a predictive model for residual stress and residual curvature in steel strips during the leveling process based on Euler–Bernoulli beam theory by introducing a mixed hardening model and improved contact characteristics. Xue et al. [10] refined the analytical model for three-dimensional elastoplastic leveling bending of steel plates based on curvature integral theory, providing calculation formulas for residual stress and residual curvature. Yi et al. [11,12], on the other hand, established a curvature-coupled model for the elastoplastic deformation of sheet metal during multi-roll leveling and further proposed evaluation criteria and analytical models for residual stress.

In the field of numerical simulation, the finite element method has become a key tool for studying complex roll systems and nonlinear behavior. Morris et al. [13,14] conducted 16 sets of finite element simulations to quantitatively analyze the effects of parameters such as roll wrap angle and leveling speed on leveling quality in a five-roll leveling model. Based on a finite element model of an 11-roll leveling mill for medium- and heavy-gauge plates, Gong et al. [15] simulated and analyzed the variation patterns of cross-sectional stress under different reduction schedules, proposing that appropriately adjusting the reduction ratio of the first roll can improve stress distribution and enhance plate flatness. Sun et al. [16] used ABAQUS/Explicit to analyze the effects of bending during the leveling process of 6 mm steel plates through a 17-roll straightener on plate shape quality and residual stress. Grüber et al. [17–19] established a numerical model of a seven-roll leveling machine using the finite element method (FEM) and systematically analyzed the influence of reduction ratio on residual stress and flatness through simulation and experiments. Gribkov et al. [20] used ABAQUS CAE analysis to study the influence of different reduction schedules on sheet quality during the leveling process, thereby determining the optimal working roll positions. Ye et al. [21] established a finite element model of an 11-roll leveling machine based on a bilinear hardening material model. Combining theoretical calculations with on-site process data, they used simulation to compare and analyze the mechanisms by which different reductions affect residual stress and flatness. Wang et al. [22,23] developed a constitutive model capable of simultaneously describing material anisotropy and the Bauschinger effect and provided a quantitative process window for the leveling of high-strength steel through system simulation. Guo et al. [24] used ANSYS Workbench finite element software to simulate the effect of leveling speed on residual stresses in heavy rails after leveling.

In recent years, research on modeling methods for leveling processes has moved beyond traditional analytical and experimental approaches, gradually shifting toward intelligent algorithms such as neural networks and deep learning, and has become a common tool for accurately predicting complex process parameters. To overcome the limitations of traditional curvature integration methods in terms of computational efficiency and convergence, Wang et al. [25] developed a prediction model for leveling force and residual curvature ratio that integrates genetic algorithms and neural networks for the 11-roll sheet leveling process. Compared to traditional models, this method improves prediction accuracy and computational efficiency. Also targeting the 11-roll leveling process, Nan et al. [26] proposed a process parameter prediction model based on the Sine-SSA-BP neural network algorithm. Compared to the BP model and the SSA-BP model, this model exhibits higher prediction accuracy and robustness. Hu et al. [27] introduced beetle optimization into the traditional BP neural network model to establish a DBO-BP-based leveling process prediction model, thereby improving the prediction accuracy of total leveling force and head-to-tail reduction.

Overall, existing research has two shortcomings: first, research has primarily focused on advanced high-strength steels with tensile strengths below 1000 MPa. Since the mechanical response and energy distribution during the leveling process of ultra-high-strength

steels undergo fundamental changes, existing simulation models are not applicable to ultra-high-strength steels with tensile strengths ≥1380 MPa (such as MS1500). Consequently, there is a lack of systematic research on their specific mechanical behavior and process windows during leveling. Second, existing research on leveling processes has largely focused on improving a single quality objective. Although some studies have begun to address energy-related parameters such as leveling force and torque, these are mostly treated as constraints or secondary objectives. Consequently, the multi-objective Pareto front is typically flat and continuous, leaving ample room for process adjustment trade-offs. In contrast, multi-objective process optimization for ultra-high-strength steels is prone to getting stuck in local optima, and there is a lack of theoretical methods and technical pathways to achieve balanced optimization.

Therefore, this paper takes 3 mm thick MS1500 ultra-high-strength steel plates produced by a certain steel mill as the subject of study. It explores an "energy–quality balanced" optimization method for multi-roll leveling processes applicable to ultra-high-strength steel, reveals the intrinsic mapping relationships between process parameters and multiple response objectives, and establishes a set of intelligent control strategies capable of adaptive adjustment based on the condition of incoming material. This holds significant theoretical importance and addresses urgent engineering needs for overcoming the current technical bottlenecks in high-precision leveling of ultra-high-strength steel plates, thereby promoting the development of leveling processes toward greater intelligence, efficiency, and environmental sustainability.

2. Energy–Quality Balance in Multi-Roll Leveling

2.1. The Essence of Energy–Quality Balance

As shown in Figure 1a, let the initial wave height of the strip be w_0; the corresponding initial curvature $\kappa_0^{(2)}$ at the exit of the first leveling unit is calculated as:

$$\kappa_0^{(2)} = \frac{2w_0}{{w_0}^2 + {L_0}^2/4}, \tag{1}$$

where w_0 is the initial wave height of the arc-shaped defect; L_0 is the chord length of the arc-shaped defect.

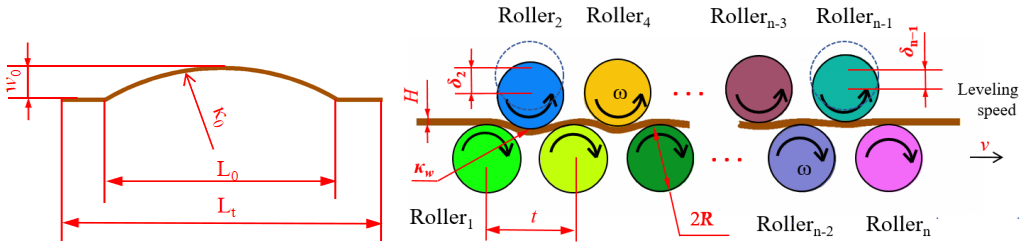


Figure 1. Leveling Process Model for Ultra-High-Strength Steel Plates: (**a**) Schematic Diagram of Initial Shape Defects in Strip Material; (**b**) The Diagram of the Multi-Roll Leveling Process.

As shown in Figure 1b, in the multi-roll leveling process, the reduction δ is the most critical control variable. According to the theory of elastoplastic bending, the steel strip undergoes reciprocating bending under the action of the leveling rolls, and the reduction directly determines the reverse curvature κ_w at each roll [9], as shown in Equation (2).

$$\kappa_w = \frac{16\delta}{4\delta^2 + t^2 - 8H\delta}, \tag{2}$$

where δ is the reduction amount of the current roll; t is the roll pitch (mm); H is the sheet thickness.

The leveling speed v determines the average single-roll plastic strain rate $\dot{\varepsilon}$ of the strip material. By coupling the above reverse curvature κ_w with the initial curvature κ_0 (the initial curvature of the incoming material for the first roller in the upper row, and the residual curvature at the exit of the previous roller for subsequent rollers) and the leveling speed, it can be calculated using Equation (3).

$$\begin{gathered}\dot{\varepsilon}(z) = g(v,z) = \left(\psi(v,z)\cdot(\kappa_w+\kappa_0) - \tfrac{\sigma_0}{E}\right)/\left(\tfrac{t}{2v}\right) = \\ \left(z\cdot\left(1-e^{-v_0/v}\right)\cdot(\kappa_w+\kappa_0) - \tfrac{\sigma_0}{E}\right)/\left(\tfrac{t}{2v}\right),\end{gathered} \tag{3}$$

where $\psi(v,z)$ is the effective arm length, which depends on the plate thickness and leveling speed; z is the distance from the neutral plane of the cross-section; v_0 is the critical speed of the material; σ_0 is the quasi-static yield strength; E is the elastic modulus of the strip material.

The strain-rate-sensitive elastoplastic stress distribution in the thickness direction is given by Equation (4).

$$\sigma(z) = \sigma_f\cdot\left(1+\left(\frac{\dot{\varepsilon}}{D}\right)^{\frac{1}{p}}\right), \tag{4}$$

where σ_f is the flow stress generated under quasi-static deformation; D is the material's strain rate coefficient; p is the strain rate exponent.

Integrating this stress distribution over the cross-sectional height yields the leveling bending moment M at this roller, which is:

$$M = \int_{-H/2}^{H/2}\sigma(z)\cdot z\,dz, \tag{5}$$

The residual curvature κ_r on the exit side was derived from Equation (6) in accordance with the unloading springback criterion.

$$\kappa_r = \kappa_w - \frac{M}{EI}, \tag{6}$$

After unloading, the elastic rebound strain κ_f at different locations along the cross-section can be expressed as:

$$\kappa_f(z) = z\cdot(\kappa_r - \kappa_w), \tag{7}$$

The residual stress field $\sigma_{res}(z)$ in the cross-section after the roller has acted can be determined as:

$$\sigma_{res}(z) = \sigma(z) + E\cdot\kappa_f(z), \tag{8}$$

The single-roll elastoplastic bending model described above serves as the state transfer element for the entire multi-roll leveling process.

By iteratively applying Equations (2)–(8) to each roll up to the final roll (the (n − 1)th roll), one can obtain the sequences of leveling bending moments $\{M_i\}_{i=2}^{n-1}$, residual curvature $\left\{\kappa_{res}^{(i)}\right\}_{i=2}^{n-1}$, and residual stress fields $\left\{\sigma_{res}^{(i)}(z)\right\}_{i=2}^{n-1}$ for each roll.

Due to their extremely high yield strength and yield-to-tensile strength ratio, the optimization of the leveling process for ultra-high-strength steel should not focus solely on quality metrics nor one-sidedly pursue energy savings; rather, it should seek a balance between "energy" and "quality." In this paper, "energy" is defined as the mechanical energy consumed during the leveling process, approximated as the integral of the drive torque of each leveling roll over the angular displacement. "Quality" is defined as the flatness

quality of the strip after leveling, which is divided into direct flatness quality and indirect flatness quality. The direct flatness quality refers to the flatness deviation after leveling, while the indirect flatness quality is represented by the peak residual stress difference (i.e., the maximum value of the range of residual stresses across all cross-sections along the strip's longitudinal direction). The mechanical energy consumption in the leveling process is expressed as:

$$P = \sum_{i=1}^{n} M_i \omega \frac{L_t}{v} = \frac{L_t}{R + H/2} \sum_{i=1}^{n} M_i \,, \tag{9}$$

where ω is the angular velocity of the working roll; L_t is the length of the strip to be leveled; R is the radius of the leveling roll.

The flatness after leveling is calculated based on the residual curvature of the final leveling unit, which is the height of the curvature per meter of chord length, expressed as:

$$\lambda = \left| \frac{1}{\kappa_{res}^{(n-1)}} \right| - \sqrt{\left(\frac{1}{\kappa_{res}^{(n-1)}} \right)^2 - 500^2} \,, \tag{10}$$

Calculation of indirect flatness quality based on the residual stress field in the final leveling unit.

$$\Delta\sigma_{max} = \left(\sigma_{res}^{(n-1)}(z)_{max} - \sigma_{res}^{(n-1)}(z)_{min} \right)_{max} \,, \tag{11}$$

"Balance" refers to achieving a joint optimization of energy consumption metrics and flatness quality (the direct and indirect flatness quality) by optimizing key process parameters—such as reduction and leveling speed—while meeting process requirements (flatness specifications after leveling).

2.2. The Impact of Key Factors on Energy–Quality and Constraints

As can be seen from the above, in the multi-roll leveling process for ultra-high-strength steel, the reduction δ, leveling speed v, and initial wave height w_0 are the key factors affecting leveling energy consumption P, post-leveling flatness λ, and the peak residual stress difference $\Delta\sigma_{max}$.

The reduction ratio δ directly affects the reverse curvature $\kappa_w^{(i)}$ at each leveling roll, which in turn influences the bending moment M_i and residual curvature $\kappa_{res}^{(i)}$. As the reduction increases, the reverse curvature increases, and the bending moment at each roll rises. As shown in Equation (9), the total mechanical energy consumption P increases monotonically accordingly. According to Equation (10), the post-leveling flatness λ is determined by the residual curvature $\kappa_{res}^{(n-1)}$ at the exit end. When the reduction is too small, plastic deformation is insufficient, resulting in a large residual curvature; when the reduction is too large, excessive bending and reverse residual curvature occur, which similarly increase the flatness deviation. There exists an optimal reduction value at which the residual curvature approaches zero; at this point, the post-leveling flatness λ deviation is minimal and exhibits a nonlinear relationship with δ, first decreasing and then increasing. According to Equation (8), the peak residual stress difference $\Delta\sigma_{max}$ stems from the non-uniform distribution of plastic strain across the cross-section $\sigma_{res}(z)$. When the reduction is too low, the proportion of the elastic zone in the cross-section is large, and the stress gradient is not pronounced; when the reduction is too high, the difference in plastic strain between the inner and outer surfaces increases, exacerbating the non-uniform distribution of residual stresses. Similarly, there exists an optimal reduction that minimizes this residual stress difference.

From Equations (3) and (4), the leveling speed affects the dynamic flow stress by altering the average single-roll plastic strain rate, thereby changing the bending moment, residual curvature, and residual stress field. Across the entire range of leveling speeds v, $\dot{\varepsilon}$ first increases and then decreases; within the practical leveling speed range ($v > v_0$), $\dot{\varepsilon}$ decreases monotonically as v increases, the bending moments at each roll decrease, and the total energy consumption P decreases; when $v \gg v_0$, $\dot{\varepsilon} \approx \frac{2\sigma_0}{Et} v$, the flow stress tends toward its static value. Therefore, P decreases as v increases, and the rate of decrease gradually slows down. According to Equations (6) and (10), the bending moment decreases as v increases, and the residual curvature decreases accordingly, resulting in improved apparent strip flatness. The applied stress field decreases overall as v increases, and the springback strain decreases; however, the combined effect of these two factors is negligible. Therefore, the peak residual stress difference is insensitive to the leveling speed.

From Equation (1), it follows that as the initial wave height w_0 increases, the initial curvature $\kappa_0^{(2)}$ of the sheet increases, the total deformation curvature $(\kappa_w + \kappa_0)$ of the first leveling unit increases, the bending moment increases, the residual curvature of subsequent rolls increases, and the bending moment of each roll increases. Consequently, as the initial wave height increases, the energy consumption of the leveling process increases monotonically. The more severe the defects in the incoming material, the less sufficient the plastic deformation under the same reduction process conditions, resulting in a larger residual curvature $\kappa_{res}^{(n-1)}$ at the exit and a deterioration in the visible flatness quality after leveling [28]. Due to the material's extremely high yield strength, the increase in bending moment caused by the initial wave height accounts for a very small proportion of the enormous bending moment required to yield ultra-high-strength steel, and is insufficient to significantly alter the stress distribution gradient in the cross-section; therefore, the peak residual stress difference exhibits low sensitivity to the initial wave height.

In summary, while increasing the reduction ratio can improve post-leveling sheet flatness and residual stress distribution, it leads to higher energy consumption during leveling; moreover, an excessive reduction ratio causes over-leveling, which degrades leveling quality. Increasing the leveling speed helps improve visible sheet flatness and reduce energy consumption but has a limited effect on latent sheet flatness quality. Initial wave height, as an input constraint, further raises the energy consumption baseline and narrows the process window. Excessive reduction in energy consumption results in insufficient leveling, while excessive focus on quality leads to a sharp increase in energy consumption and a deterioration in quality. Therefore, within the constraints of the process feasibility domain, it is essential to optimize the coupling between reduction ratio and leveling speed to achieve a controlled trade-off between energy consumption and quality metrics, thereby realizing the balanced optimization of both.

3. Finite Element Modeling and Experimental Design for Multi-Roll Leveling of UHSS

Due to the highly nonlinear and multivariable coupled nature of the ultra-high-strength steel leveling process, it is difficult to derive analytical relationships between the various objectives, constraints, and decision variables. This paper employs finite element simulation and surrogate modeling methods. Taking the 17-roll UHSS leveling process as an example, a finite element model of the leveling process was established using Abaqus/Explicit 2021. The leveling machine roller system adopts an upper-eight, lower-nine configuration; specific parameters are shown in Table 1.

Table 1. Working parameters of the leveler.

Parameters	Value
Number of work rollers	17 (top: 8, bottom: 9)
Roller diameter/mm	100
Roller pitch/mm	110
Allowable total leveling force/kN	25,000
Motor power/kW	205
Top Roll Vertical Adjustment Stroke/mm	100
Width of plate/mm	1200
Yield Strength of steel strip/MPa	<1700
Leveling speed/m·min^{-1}	≤7.5

3.1. Finite Element Modeling and Parameter Settings for the Leveling Process

The subject of this study is a 1500 mm × 1000 mm × 3 mm MS1500 martensitic ultra-high-strength steel plate provided by a certain company. The Chaboche nonlinear mixed hardening model is adopted in this paper to characterize the cyclic hardening behavior of the material. Combining isotropic and kinematic hardening, the model effectively captures the Bauschinger effect. In Abaqus/Explicit, it is activated via the "Hardening = Combined" option, with the corresponding parameters specified directly in the material definition. Its basic physical properties and the parameters of the mixed hardening constitutive model [29] are listed in Tables 2 and 3, respectively. To quantify the strain rate effect, this study adopted the Cowper–Symonds model to account for dynamic strengthening behavior [30] and conducted uniaxial tensile tests at different strain rates. The strain rate coefficient D and the strain rate exponent p of this model, obtained by fitting the experimental results, are also listed in Table 3. The following simplifications and parameter settings were applied during the modeling process:

Table 2. Basic Mechanical Properties of MS1500 Steel.

Parameters	Young's Modulus/MPa	Yield Strength/MPa	Tensile Strength/MPa	Elongation/%
Value	203,049.76	1330	1576	8.86

Table 3. Parameters for the Combined Hardening Constitutive Model of Sheet Metal.

Parameters	C_1/MPa	C_2/MPa	C_3/MPa	γ_1	γ_2	γ_3	Q/MPa	b	D	p
Value	1316.2	11,407.3	16,187.9	1	72.5	295.8	200.1	291.9	618.24	20.36

(1) Variations in wave height across the plate's width were neglected, and the plate was set as a 2D initial plate shape with three curvature features.
(2) The leveling rolls were treated as rigid bodies, while the plate was defined as a deformable body.
(3) For room-temperature leveling, the CPS4R element with reduced integration and hourglass control was adopted. A mesh sensitivity study using coarse (2400), medium (5000), and fine (7500) elements yielded roll-force errors of 7.12%, 4.23%, and 3.93%, respectively, against experiments. The medium mesh (10 layers, 3 mm) was adopted for all subsequent simulations, balancing accuracy and computational cost.
(4) Surface-to-surface contact was defined between the plate and the rolls, with the penalty method for tangential behavior (friction coefficient = 0.2, constant) and hard contact for normal behavior.

The leveling process was carried out in three analysis steps: step 1, initial leveling conditions were established, including the roll compression action of the upper row of

leveling rolls and the roll reduction settings; step 2 applies an initial velocity to the sheet to ensure its stable "engagement" into the leveling zone; step 3, after the sheet has "engaged," releases the previously applied velocity load, with subsequent motion driven by friction between the leveling rolls and the steel sheet.

3.2. Verification of Finite Element Models

Finite element models of leveling processes are typically validated using the total leveling force as a key metric [21,31,32]. In this study, a laser flatness measuring instrument was used to measure the initial wave height of the sheet [33]. The measured analysis of the sheet's morphology revealed a typical mid-section convex wave defect: the wave region was concentrated within a range of approximately 500 mm in the center of the sheet, with the initial wave height distributed between 10.5 and 14.6 mm. Three sheets with typical initial wave heights—11.10 mm, 12.30 mm, and 14.20 mm—were selected. Simulation and leveling experiments were conducted using a leveling speed of 7.500 m·min^{-1}, an entry reduction of 2.750 mm, and an exit reduction of 2.250 mm. The simulation data was analyzed to directly extract the leveling forces of each roller in the upper roll set, and the resultant force was calculated as the total simulated leveling force. Figure 2 shows the simulation results for the leveling of a strip with an initial wave height of 12.3 mm: the residual stress contour plot in Figure 2a illustrates the stress stratification characteristics within the cross-section of the sheet after straightening; Figure 2b shows the time-history curves of the straightening forces for each roller in the upper roll set, clearly illustrating the evolution of individual roller loads over time and providing a basis for the quantitative calculation of the total straightening force.

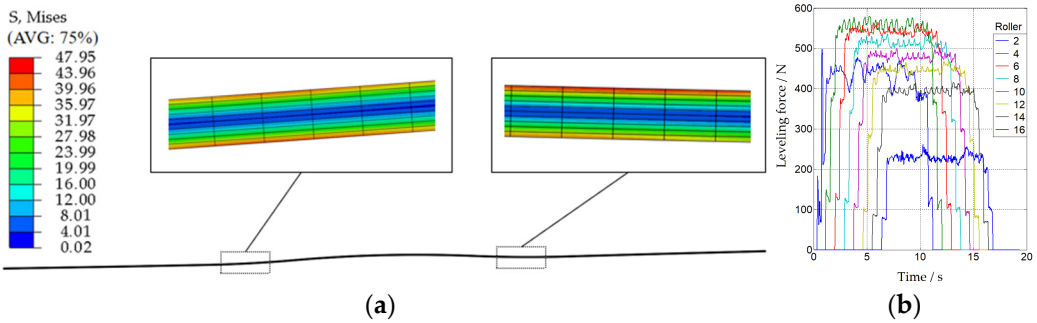


Figure 2. Post-leveling results of a strip with an initial wave height of 12.3 mm: (**a**) Nephogram of residual stress after leveling; (**b**) Upper row roll leveling forces.

The deformation of the column was monitored in real time using a magnetostrictive linear displacement sensor (AMT Sensor Company, Nanjing, China) mounted on the operating-side column of the stand. By combining this data with the deformation of the sheet's centerline as it reached the 9th roll, the stiffness of the stand on the entry and exit sides was calculated based on the cross-sectional dimensions of a single column. The sum of the forces on both sides was then calculated to determine the measured total leveling force (as shown in Figure 3). A comparison of the simulated and experimental total leveling force data is presented in Table 4.

Although the simulation results for one set of scenarios were slightly higher than the experimental values due to the influence of coupled factors—such as simulation errors in the roll-sheet contact boundary conditions, the neglect of initial internal residual stresses in the sheet, and differences in the stiffness of the actual equipment—the error between the experimental and simulated values for all scenarios remained within 6%, indicating that the deviations were still within an acceptable range. The high degree of agreement between the two sets of data indicates that the constructed model effectively captures the mechanical behavior of the actual leveling process for ultra-high-strength steel. Therefore,

the finite element model developed can be used to analyze the evolution of flatness, residual stress, and leveling energy consumption in the multi-roll leveling process of ultra-high-strength steel.

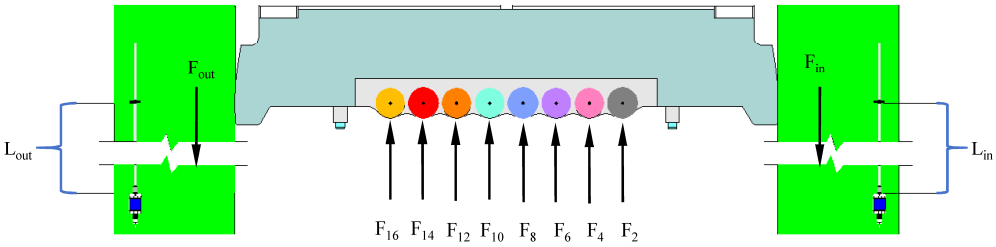


Figure 3. The structural drawing of an upper leveling roller.

Table 4. Comparison of Leveling Forces between Simulation and Experiment.

Initial Wave Height/mm	Experimental Leveling Force/KN	Simulated Leveling Force/KN	Error/ %
11.10	1251	1179.97	5.68
12.30	1185	1198.90	1.17
14.20	1141	1093.32	4.18

3.3. Virtual Experiment Design Proposal

Based on a comprehensive analysis of on-site process parameters and measured data on initial sheet defects, reasonable ranges for each design variable were determined. Specifically, based on the statistical characteristics of incoming sheet flatness defects observed in actual production, the initial wave height was set at 10.5–14.6 mm. In the multi-roll leveling process, the total reduction must be distributed among the individual leveling rolls [28]. Most existing multi-roll levelers feature linear reduction in the upper rolls, with the entry zone performing primary plastic deformation and the exit zone for plate shape fine-tuning. To accurately represent the leveling process and capture the effect of reduction distribution on leveling outcomes, the reduction is defined as two independent design variables: entry reduction and exit reduction. Based on on-site operating records and references [28,32], the following values were determined: the entry reduction is 2.50–3.00 mm, and the exit reduction is 2.00–2.50 mm. Based on the capacity of the on-site leveling machine, its maximum operating speed is 7.5 m·min^{-1}. Considering the balance between production efficiency and leveling quality and referencing on-site equipment operation records, the leveling speed range was set to 2.5–7.5 m·min^{-1}, covering the equipment's commonly used speed range.

To investigate the influence of the aforementioned design variables on post-leveling plate shape and energy consumption indicators, the Box–Behnken experimental design method was adopted to construct a simulation test set with four factors and three levels, generating a total of 27 simulation scenarios. The coding levels for each parameter are listed in Table 5, and the complete test combinations along with their finite element simulation results are summarized in Table 6.

Table 5. Table of factor levers.

Level	Experimental Factors			
	X_1: Initial Wave Height /mm	X_2: Entry Reduction /mm	X_3: Exit Reduction /mm	X_4: Leveling Speed /m·min^{-1}
−1	10.50	2.50	2.00	2.5
0	12.55	2.75	2.25	5.0
1	14.60	3.00	2.50	7.5

Table 6. Test result.

Sample No.	Factors and Level				Response Value		
	X_1 /mm	X_2 /mm	X_3 /mm	X_4 /m·min^{-1}	Leveling Energy/mJ	Flatness/mm·m^{-1}	Peak Residual Stress Difference/MPa
1	14.60	3.00	2.25	5.0	282,286	−6.04528	166.635
2	12.55	2.75	2.00	7.5	162,115	−5.62163	141.788
3	10.50	2.75	2.50	5.0	281,536	−6.85723	113.371
4	14.60	2.75	2.25	2.5	531,382	−7.61274	159.410
5	14.60	2.75	2.25	7.5	172,323	−5.56089	153.798
6	10.50	2.5	2.25	5.0	252,451	−9.59939	56.0971
7	12.55	2.75	2.50	2.5	562,440	−7.13905	133.221
8	12.55	3.00	2.25	2.5	558,337	−7.47357	152.224
9	10.50	3.00	2.25	5.0	280,626	−4.70832	140.814
10	14.60	2.50	2.25	5.0	247,327	−11.1721	86.9717
11	14.60	2.75	2.50	5.0	281,627	−8.10949	154.432
12	14.60	2.75	2.00	5.0	251,149	−8.28796	160.372
13	12.55	2.50	2.50	5.0	266,038	−10.2981	92.6021
14	12.55	3.00	2.25	7.5	181,418	1.69584	152.856
15	12.55	2.75	2.00	2.5	501,830	−5.87071	142.309
17	12.55	2.50	2.00	5.0	232,281	−10.8727	54.5636
18	12.55	2.75	2.25	5.0	264,260	−7.44727	131.147
19	12.55	3.00	2.50	5.0	290,384	−6.69959	158.310
20	12.55	2.75	2.25	5.0	264,260	−7.44727	131.147
21	12.55	3.00	2.00	5.0	265,537	−5.48509	158.920
22	10.50	2.75	2.00	5.0	252,864	−6.91347	124.459
23	12.55	2.50	2.25	7.5	162,450	−9.61742	73.1139
24	12.55	2.75	2.50	7.5	183,163	−4.56712	134.133
25	10.50	2.75	2.25	2.5	532,314	−6.94377	108.043
26	10.50	2.75	2.25	7.5	176,859	−3.51189	116.826
27	12.55	2.50	2.25	2.5	501,796	−7.44814	73.0203

4. Response Surface Modeling and Multi-Objective Response Analysis

4.1. Building a Response Surface Modeling Agent

Based on the experimental data in Table 6, Design-Expert 13 was used to perform regression modeling on the three response variables—leveling energy consumption, post-leveling flatness, and peak residual stress difference—using the least squares method. For each response variable, linear models, second-order interaction models (2FI), quadratic polynomial models, and cubic models were fitted sequentially. The suitability of the different models was systematically evaluated based on the probability *p*-values, calibration coefficients $R_a{}^2$, and prediction coefficients $R_p{}^2$ output by each model, as shown in Table 7. Through comparative analysis, the quadratic polynomial model yielded a significant *p*-value and demonstrated a high degree of goodness of fit.

Response relationship models were established between leveling energy consumption, post-leveling flatness, and peak residual stress difference and various factors. These models were fitted at a 95% confidence level as shown in Equations (12)–(14), with determination coefficients of 99.97%, 97.63%, and 97.79%, respectively.

$$\begin{aligned} Y_1 = 186499 &- 22222.68804X_1 + 248377X_2 + 198844X_3 - 132358X_4 + 3309.24464X_1X_2 + 880.90859X_1X_3 \\ &- 175.85209X_1X_4 - 35640.8928X_2X_3 - 15029.35772X_2X_4 - 15824.63124X_3X_4 + 461.76818{X_1}^2 \\ &- 12573.62167{X_2}^2 + 7490.30873{X_3}^2 + 13984.18435{X_4}^2 \end{aligned} \quad (12)$$

$$Y_2 = -64.86938 + 0.018591X_1 + 35.38836X_2 + 32.3178X_3 - 16.21303X_4 + 0.115017X_1X_2 + 0.059625X_1X_3 - 0.067319X_1X_4 - 7.15651X_2X_3 + 4.53548X_2X_4 + 0.929138X_3X_4 - 0.018645{X_1}^2 - 6.05632{X_2}^2 - 4.05283{X_3}^2 + 0.300492{X_4}^2 \quad (13)$$

$$Y_3 = -3393.59086 + 3.30663X_1 + 2315.61712X_2 + 21.80365X_3 + 4.3957X_4 - 2.46527X_1X_2 + 2.51127X_1X_3 - 0.702195X_1X_4 - 154.5916X_2X_3 + 0.21532X_2X_4 + 0.57312X_3X_4 + 0.412679{X_1}^2 - 322.44727{X_2}^2 + 82.25793{X_3}^2 + 0.267817{X_4}^2 \quad (14)$$

Table 7. Result of regression model significance analysis.

Source		Linear	2FI	Quadratic	Cubic
Leveling Energy	Sequential *p*-value	<0.0001	0.9996	<0.0001	0.0018
	${R_a}^2$	0.8627	0.814	0.9993	1
	${R_p}^2$	0.822	0.6406	0.9982	0.9994
Flatness	Sequential *p*-value	0.0003	0.042	<0.0001	0.3633
	${R_a}^2$	0.5311	0.6905	0.9486	0.9617
	${R_p}^2$	0.3766	0.3727	0.8633	0.1518
Peak residual stress difference	Sequential *p*-value	<0.0001	0.9304	0.0001	<0.0001
	${R_a}^2$	0.8193	0.7763	0.9521	0.9999
	${R_p}^2$	0.7603	0.545	0.8726	0.9988

4.2. Evaluation of Proxy Model Accuracy

Significance analysis of the models indicates that all *p*-values are less than 0.0001, indicating extremely high overall model significance [34] and strong statistical reliability. As shown in Table 8, a comprehensive evaluation of the reliability of each model reveals that all correlation coefficients R^2 exceed 0.97, indicating a high degree of agreement between predicted and experimental values; the model prediction coefficients ${R_p}^2$ are all greater than 0.86, and the differences from the calibration coefficients ${R_a}^2$ are all less than 0.1, indicating a high degree of fit and stable performance [35]; the coefficient of variation (C.V.) for all models is below 10%, and the Adeq Precision (signal-to-noise ratio) is far greater than 4, thus demonstrating high accuracy and reliability.

Table 8. Result of model reliability tests.

Regression Model	R^2	${R_a}^2$	${R_p}^2$	C.V./%	Adeq Precision	*F*-Value	*p*-Value
Y_1	0.9997	0.9993	0.9982	1.10	157.3300	2817.23	<0.0001
Y_2	0.9763	0.9486	0.8633	8.33	27.5595	35.26	<0.0001
Y_3	0.9779	0.9521	0.8726	5.78	21.9560	15.67	0.0001

To verify the model's generalization capability, eight additional independent validation experiments were conducted within the design ranges of each factor. These eight new experimental points covered both the boundaries and the central region of the design domain and were uniformly distributed within the process parameter space. The specific parameters of the validation points, along with the RSM predictions and FE simulation results, are compared in Table 9.

Figure 4 shows that the predicted and simulated values for the three responses in the validation experiment are closely distributed on both sides of the 45° reference line, demonstrating good agreement. Within the established design space, the response surface models can effectively replace finite element simulations for rapid prediction, exhibiting favorable fitting accuracy and generalization capability. Hence, they are well-suited for subsequent analysis and optimization.

Table 9. FE simulation and RSM prediction results of the Validation Group.

Sample No.	Factors and Level				FEM Results/RSM Prediction Values		
	X_1 mm	X_2 mm	X_3 mm	X_4 m·min^{-1}	Y_1/J	Y_2/mm·m^{-1}	Y_3/MPa
N1	11.30	2.60	2.40	6.0	198.4/209.2	−8.726/−8.305	95.29/94.51
N2	13.80	2.90	2.10	3.5	397.9/404.5	−7.042/−7.181	167.13/166.49
N3	12.00	2.75	2.25	4.5	290.9/303.9	−7.679/−7.467	122.28/126.11
N4	14.00	2.50	2.30	5.5	209.4/219.1	−10.896/−11.106	85.44/86.72
N5	10.80	3.00	2.00	7.0	182.6/180.6	−0.277/−0.289	160.52/157.89
N6	12.80	2.65	2.10	6.5	182.0/176.8	−7.947/−8.249	111.18/113.47
N7	11.50	2.90	2.35	3.0	495.2/486.9	−7.399/−7.436	133.73/137.42
N8	13.20	2.50	2.15	5.0	244.1/239.0	−11.037/−10.797	75.32/72.99

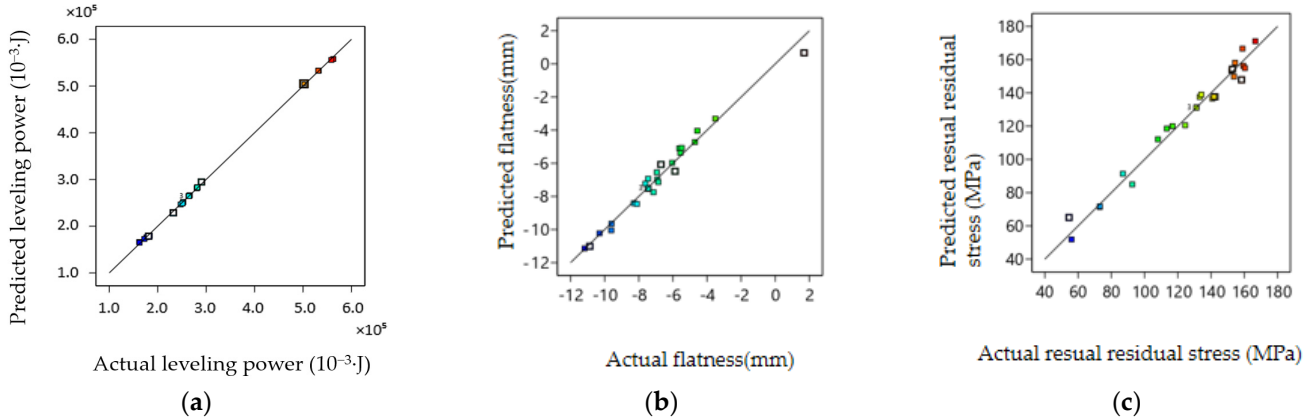


Figure 4. Comparison of Simulation and Prediction Results in the Validation Group: (**a**) The leveling energy consumption; (**b**) The post-leveling flatness; (**c**) The peak residual stress difference.

4.3. Analysis of Key Factors' Effects on Energy–Quality Indicators

Leveling speed X_4 is the primary determinant of leveling energy consumption (Y_1) and exhibits a significant interaction with the reduction ratio, as shown in Figure 5. The low ductility of ultra-high-strength steel makes its energy consumption extremely sensitive to leveling speed. At lower leveling speeds, energy consumption increases monotonically with increasing reduction; at higher leveling speeds, however, the increase in energy consumption resulting from the same increment in reduction is much more gradual. A process with higher leveling speeds not only helps reduce leveling energy consumption but also mitigates the negative impact of changes in reduction on energy consumption. The initial wave height X_1 is a secondary factor affecting leveling energy consumption; its effect is relatively independent of other process parameters, and its interactions with each parameter are not significant.

Leveling speed X_4 is the dominant factor affecting post-leveling flatness Y_2, followed by entry reduction X_2, while exit reduction X_3 has a relatively weaker influence. A leveling speed of $X_4 > 5.0$ m·min^{-1} can effectively suppress springback in ultra-high-strength steel, promote stress homogenization, and significantly improve sheet flatness. As shown in Figure 6, there is a significant interaction effect between the entry reduction ratio and leveling speed; increasing X_2 at higher speeds can substantially reduce flatness, whereas the effect is limited at low speeds. The interaction between the exit reduction ratio and leveling speed is nonlinear; when the leveling speed exceeds 5.0 m·min^{-1}, increasing X_3 improves post-leveling sheet quality, whereas the opposite is true at low speeds. Increasing the leveling speed helps overcome the strong springback tendency of ultra-high-strength steel materials and enhances their plastic flow and cumulative effect under alternating bending. The effect of initial wave height X_1 on post-leveling flatness exhibits significant

interaction dependence—its interaction with both entry reduction X_2 and exit reduction X_3 is relatively weak, but it shows a significant interaction with leveling speed X_4. Under high leveling speed conditions, increasing the initial wave height X_1 leads to a significant deterioration in post-leveling flatness.

The entry reduction X_2 and exit reduction X_3 are key parameters for controlling the distribution of residual stresses, and they interact significantly with the peak residual stress difference Y_3, as shown in Figure 7. The high yield strength of ultra-high-strength steel results in high deformation resistance; the entry reduction directly determines the extent of initial plastic deformation and is the primary source of residual stresses. The interaction between X_2 and X_3 is opposite in direction: when the entry reduction is low, the cumulative plastic strain introduced by preceding passes is limited, and the cyclic softening effect of the material has not yet been fully activated. Increasing the exit reduction introduces additional reverse plastic deformation in the final pass—due to the Bauschinger effect, which lowers the reverse yield stress, deformation tends to concentrate in localized surface regions where plasticity has already occurred, thereby exacerbating stress concentration and increasing the peak residual stress difference; whereas when the entrance reduction is high, sufficient cumulative equivalent plastic strain has already been accumulated in the preceding passes, the dislocation density within the material tends toward saturation, and dynamic recovery and dislocation annihilation processes dominate microstructural evolution, leading to a reduction in flow stress. At this point, increasing the exit reduction is equivalent to applying a controlled reverse plastic deformation in the final pass, which utilizes the already activated cyclic softening state to effectively release the residual stresses accumulated in previous passes—the exit reduction thus acts as a "regulator" for residual stresses. The effect of leveling speed X_4 is relatively weak. An increase in X_1 directly leads to an increase in Y_3 and exhibits a significant interaction with the leveling speed X_4. Reducing the leveling speed X_4 under conditions of higher initial wave height results in a further increase in Y_3.

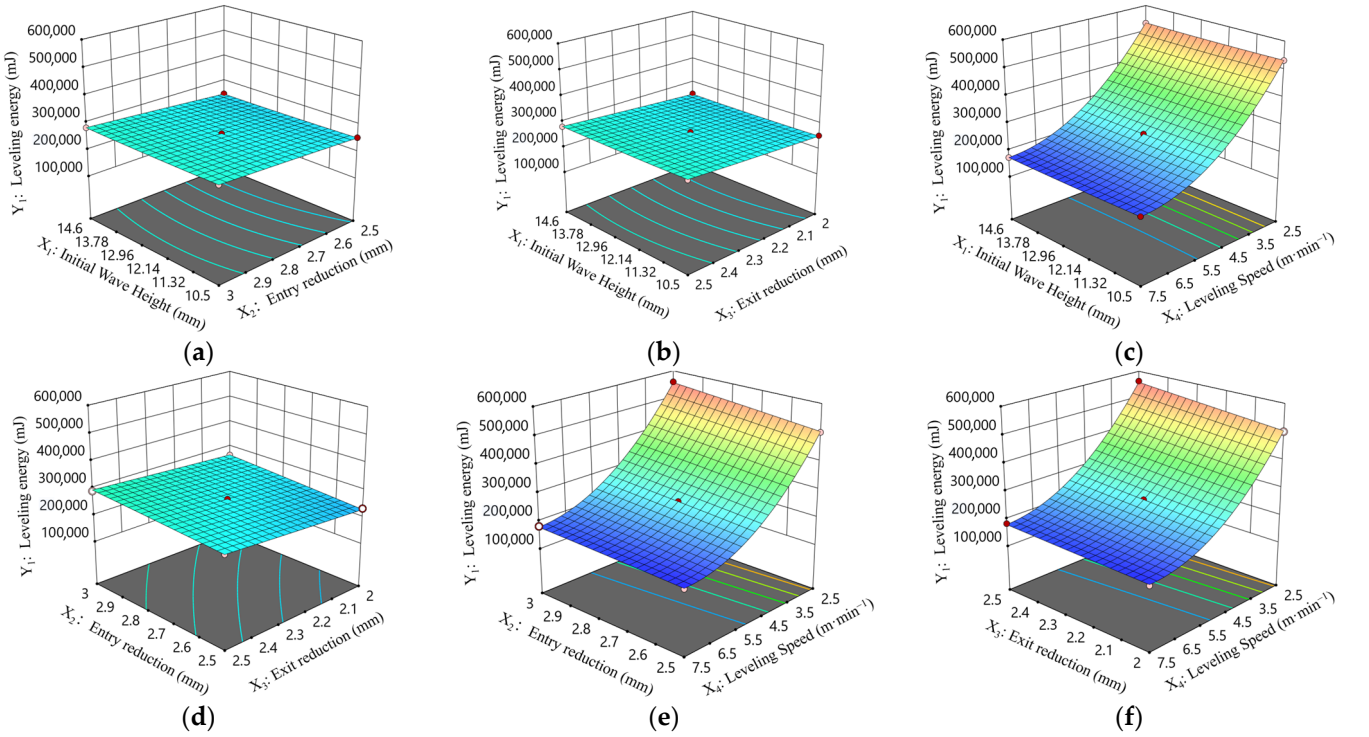


Figure 5. Response surface of Y_1: (**a**) Interaction between X_1 and X_2; (**b**) Interaction between X_1 and X_3; (**c**) Interaction between X_1 and X_4; (**d**) Interaction between X_2 and X_3; (**e**) Interaction between X_2 and X_4; (**f**) Interaction between X_3 and X_4.

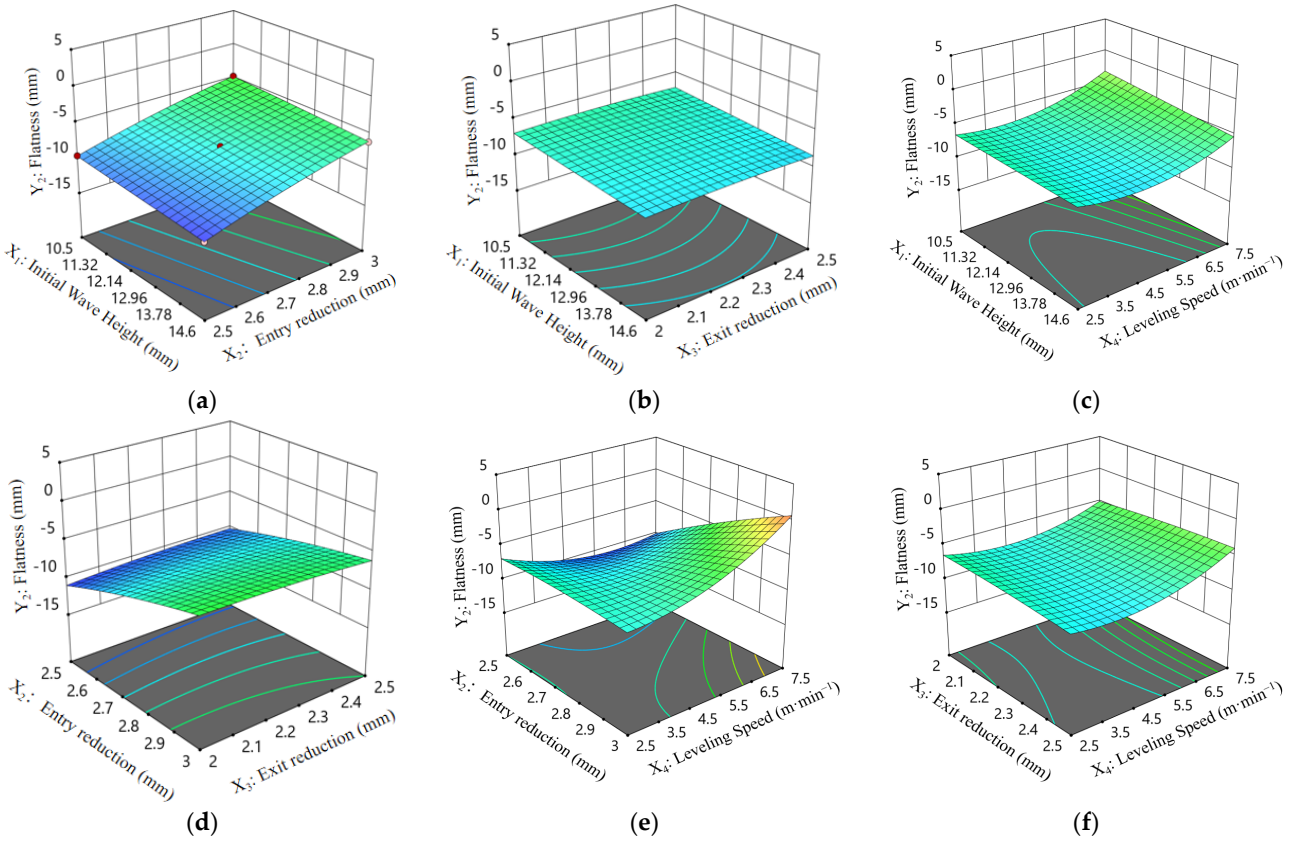


Figure 6. Response surface of Y_2: (**a**) Interaction between X_1 and X_2; (**b**) Interaction between X_1 and X_3; (**c**) Interaction between X_1 and X_4; (**d**) Interaction between X_2 and X_3; (**e**) Interaction between X_2 and X_4; (**f**) Interaction between X_3 and X_4.

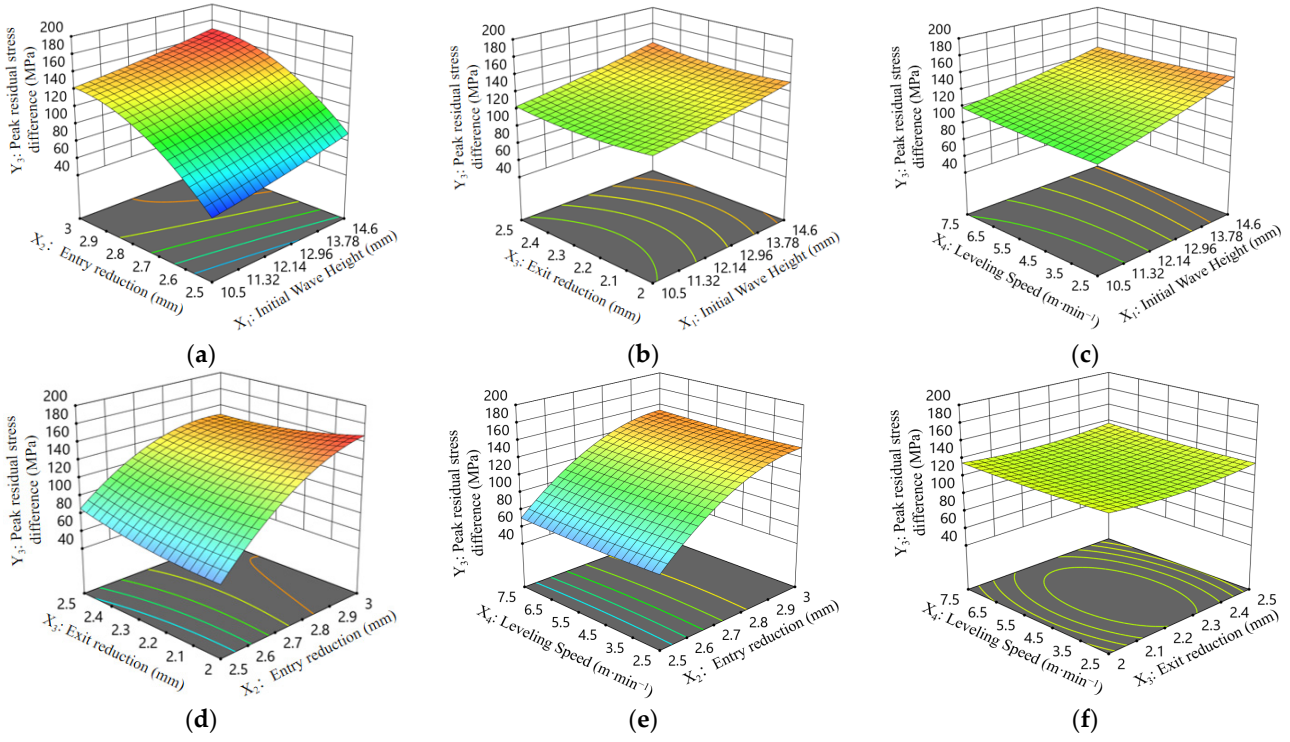


Figure 7. Response surface of Y_3: (**a**) Interaction between X_1 and X_2; (**b**) Interaction between X_1 and X_3; (**c**) Interaction between X_1 and X_4; (**d**) Interaction between X_2 and X_3; (**e**) Interaction between X_2 and X_4; (**f**) Interaction between X_3 and X_4.

The above analysis is generally consistent with the trends predicted by the theoretical model, validating the reliability of the leveling process analysis framework. Within the initial wave height range of 10.5–14.6 mm, the various responses (leveling energy consumption, post-leveling unevenness, and peak residual stress) are relatively sensitive to changes in process parameters (entry and exit reduction ratios and leveling speed), and the trade-off between energy and quality objectives is particularly pronounced. Traditional single-parameter adjustments struggle to simultaneously optimize current sheet shape and improve force–energy indicators. Therefore, constructing an energy–quality co-optimization model for the feasible domain of process parameters within this initial wave height range, and subsequently establishing adaptive process curves based on initial wave height, is the key path to overcoming the current bottlenecks in the leveling process for ultra-high-strength steel.

5. Balanced Optimization of Leveling Process Parameters for Energy and Quality

5.1. Modeling the Problem of Energy–Quality Balanced Optimization

The leveling process must simultaneously meet multiple objectives, including leveling energy consumption, post-leveling flatness, and peak residual stress difference. Since trade-offs exist among these objectives, traditional single-objective optimization struggles to achieve overall performance [36]. Based on the definition in Section 2.1, this paper sets leveling energy consumption Y_1 (reflecting "energy") and the peak residual stress difference Y_3 (reflecting "quality") as optimization objectives; furthermore, in accordance with core quality requirements for shipped products, post-leveling flatness ($|Y_2| \leq 3.50$ mm·m^{-1}), which reflects explicit sheet flatness quality, is established as a constraint. The initial waviness height X_1 is a raw material parameter and is fixed in this study; the process parameters (X_2, X_3, X_4) are treated as design variables, and the multi-objective optimization function is established as follows:

$$\min \begin{cases} f_1(X_1; X_2, X_3, X_4) = Y_1 \\ f_2(X_1; X_2, X_3, X_4) = Y_3 \end{cases}, \tag{15}$$

To ensure the engineering robustness of the optimization results and account for the model's predictive accuracy, a safety margin of 0.02 mm·m^{-1} was incorporated when defining the constraints. Specifically, the post-correction flatness constraint was set to $|Y_2| \leq 3.48$ mm·m^{-1}. The constraints are as follows:

$$s.t. \begin{cases} |Y_2| \leq 3.48 \\ X_2 \in [2.5, 3.0] \\ X_3 \in [2.0, 2.5] \\ X_4 \in [2.5, 7.5] \end{cases}, \tag{16}$$

5.2. Solving and Decision-Making on the Pareto Frontier

For the aforementioned multi-objective optimization model, the Non-dominated Sorting Genetic Algorithm II (NSGA-II) with an elite strategy was used for iterative solutions. The parameters [35,36] were set as follows: population size of 500, maximum number of iterations of 200, crossover probability of 0.8, and 20 cycles. After merging, deduplication, and non-dominated sorting, a set of Pareto-optimal solutions was obtained.

Taking an initial wave height of 10.50 mm as an example, the Pareto front generated by the optimization is shown in Figure 8. The non-dominated solutions exhibit a continuous distribution in the objective space, and the solution set covers the Pareto front relatively completely. This verifies that the algorithm is stable and capable of approximating the true

Pareto front, thereby yielding a high-quality set of non-dominated solutions. This curve also illustrates the trade-off between performance and quality; in the leveling process, it is impossible to simultaneously optimize both the peak residual stress difference and leveling energy consumption to their extremes, and there is no single global optimal solution for the process parameters. Therefore, the selection of optimal parameters constitutes a typical multi-criteria engineering decision-making problem, requiring a choice within the decision space of the Pareto solution set based on the priority order of various indicators in actual production. For the 458 process combination optimization schemes in the Pareto-optimal solution set, the TOPSIS method was employed for comprehensive evaluation and decision analysis to screen for a compromise solution. As shown in Figure 8, Region I comprises non-dominant solutions that prioritize leveling energy consumption. If the peak residual stress difference after leveling is the primary criterion, selections should be made from Region III. Region II represents the selection space for compromise solutions that balance both criteria.

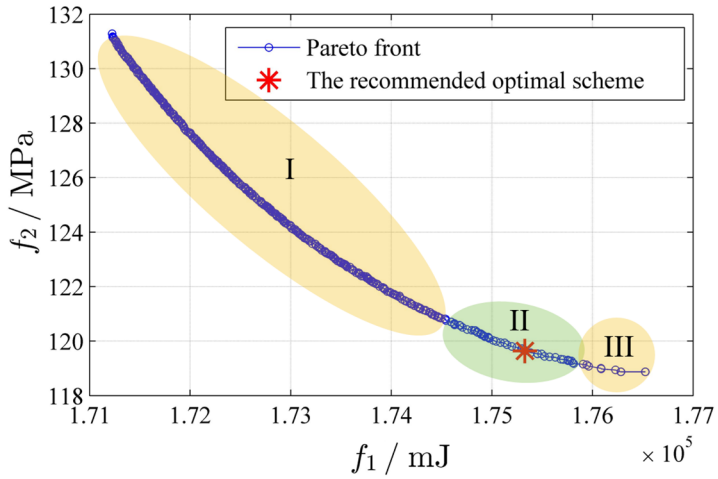


Figure 8. Pareto optimal front when X_1 = 10.5 mm.

The relative proximity [37] objectively reflects how closely each scheme approximates the ideal solution, effectively balancing the two objectives of minimizing the peak residual stress difference and reducing leveling energy consumption. The relative proximity of the various schemes is primarily concentrated in the range of 0.50–0.80, indicating the presence of multiple high-quality candidate schemes with similar overall performance. From the 458 Pareto non-dominated solutions, the top seven sets of solutions with a proximity index greater than 0.7915 are listed in Table 10. The leveling speed X_4 remains stable at around 7.5 m·min^{-1}, with negligible variation. Among these, Solution 385 has the highest relative proximity index (0.79210) and is closest to the ideal solution. Its process parameters X_2 and X_3 (2.751 mm and 2.179 mm) are both close to the median values of the corresponding parameters in other solutions, indicating better parameter robustness. Although the corresponding peak residual stress difference (119.64 MPa) is not the lowest, it differs from the lowest value (119.58 MPa for Scheme #128) by only 0.14%, and its leveling energy consumption (175,328.93 mJ) is significantly lower than that of Scheme #128, demonstrating superior load performance. Furthermore, the mean values f_1 and f_2 for the first seven groups of solutions are 175,171.73 mJ and 119.87 MPa, respectively, with relative deviations from the optimal solution of only 0.09% and 0.17%, indicating a high-density cluster of high-quality solutions near the optimal solution; The mean metrics for all 458 frontier solutions were 172,952.17 mJ and 125.12 MPa, respectively, with relative deviations from the optimal solution reaching 1.36% and 4.58%. Therefore, the TOPSIS method not only identifies the comprehensive optimal compromise point on the Pareto frontier but also ensures that this point is located within a region of high-quality solutions,

offering good tolerance for process parameter adjustments. Solution 385 was ultimately selected as the recommended optimal combination of process parameters (X_2 = 2.7469 mm, X_3 = 2.2164 mm, X_4 = 7.4987 m·min^{-1}) for the leveling process of incoming material with a wave height of 10.50 mm.

Table 10. TOPSIS Evaluation of the Top Seven Process Combinations and Their Response Indicators.

Sample No.	Relative Closeness	Factors			Response Value	
		X_2 mm	X_3 mm	X_4 m·min^{-1}	f_1/mJ	f_2/MPa
385	0.79210	2.7469	2.2164	7.4987	175,328.93	119.64
53	0.79198	2.7483	2.2035	7.4990	175,041.17	119.99
248	0.79190	2.7476	2.2104	7.4975	175,198.23	119.81
130	0.79187	2.7479	2.2083	7.4984	175,150.22	119.87
389	0.79180	2.7484	2.2023	7.4990	175,014.08	120.03
301	0.79165	2.7482	2.2053	7.4977	175,084.05	119.95
128	0.79153	2.7467	2.2189	7.4990	175,385.38	119.58

5.3. Construction of Adaptive Optimization Curves for Process Parameters in Response to Incoming Wave Heights

To achieve adaptive control of the leveling process under varying feed conditions, this paper establishes a full-process parameter recommendation mechanism tailored to the actual production range of wave height fluctuations, based on the determination of an optimal combination of process parameters for a typical initial wave height (X_1 = 10.5 mm). The initial wave height range [10.5, 14.6] mm is divided into 42 levels (with a step size of 0.1 mm) using equal spacing. For each discrete wave height $X_1^{(i)}$ (i = 1, 2, 3, . . ., 42), the collaborative optimization process is repeated: the established collaborative optimization model is invoked; within the feasible domain of process constraints, NSGA-II is used to solve for the Pareto front that minimizes both leveling energy consumption Y_1 and the peak residual stress difference Y_3; the TOPSIS method is employed to calculate relative proximity and screen for the comprehensive optimal solution, outputting the corresponding recommended process parameters ($X_2^{(i)}$, $X_3^{(i)}$, $X_4^{(i)}$). By iterating through all initial wave heights, a complete dataset of recommended process parameters is obtained. Through iterative calculations, the corresponding optimal process parameter combinations are derived. Table 11 presents the recommended process parameter combinations for selected wave heights.

Because traditional linear fitting methods struggle to account for the coupling effects among various factors, directly applying linear fitting to the dataset of optimal process parameters may result in prediction results that deviate from the true optimal process window, thereby preventing the flatness of the corrected steel plate from meeting the threshold requirement of 3.5 mm·m^{-1}. Based on the aforementioned 42 sets of optimal process parameters, this paper employs linear interpolation to determine the process parameters corresponding to the midpoints of different incoming wave heights, and plots the curves showing how each optimal process parameter varies with the initial incoming wave height (Figure 9). Analysis indicates that as the initial wave height X_1 increases, the required entry reduction X_2 correspondingly increases; the curve of the optimal parameter X_2 exhibits a monotonically increasing trend; the optimal exit reduction X_3 decreases from 2.211 mm to 2.191 mm as the initial wave height X_1 increases, exhibiting nonlinear fluctuations, with the initial wave height serving as a coordinating parameter for the adjustment of the exit reduction rather than a dominant variable; The optimal leveling speed X_4 fluctuates slightly within the range of 7.498–7.499 m·min^{-1}, and its regulatory effect on leveling quality is relatively limited; the system primarily relies on other process parameters to achieve primary control.

Table 11. The recommended process parameter combinations.

Initial Wave Height	Comprehensive Optimal Process Parameters		
	$X_2^{(i)}$	$X_3^{(i)}$	$X_4^{(i)}$
$X_1^{(2)} = 10.60$	2.74950	2.21109	7.49838
$X_1^{(5)} = 10.90$	2.75520	2.21487	7.49964
$X_1^{(8)} = 11.20$	2.76224	2.20811	7.49872
$X_1^{(11)} = 11.50$	2.76911	2.20383	7.49917
$X_1^{(14)} = 11.80$	2.77526	2.20829	7.49865
$X_1^{(17)} = 12.10$	2.78123	2.21512	7.49924
$X_1^{(20)} = 12.40$	2.78893	2.20785	7.49879
$X_1^{(23)} = 12.70$	2.79665	2.20238	7.49819
$X_1^{(26)} = 13.00$	2.80426	2.19773	7.49983
$X_1^{(29)} = 13.30$	2.81142	2.20045	7.49936
$X_1^{(32)} = 13.60$	2.81913	2.19859	7.49932
$X_1^{(35)} = 13.90$	2.82715	2.19589	7.49931
$X_1^{(38)} = 14.20$	2.83493	2.19702	7.49988
$X_1^{(41)} = 14.50$	2.84359	2.19122	7.49930

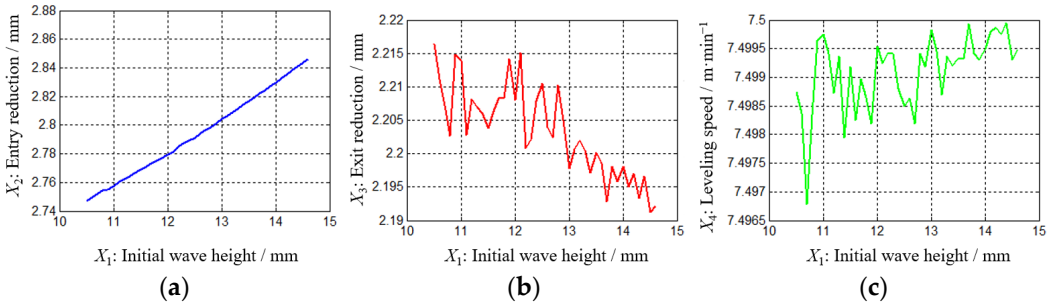


Figure 9. Relationship curves between initial wave height and each optimized process parameter: (**a**) Initial wave height X_1 vs. optimal parameter X_2; (**b**) Initial wave height X_1 vs. optimal parameter X_3; (**c**) Initial wave height X_1 vs. optimal parameter X_4.

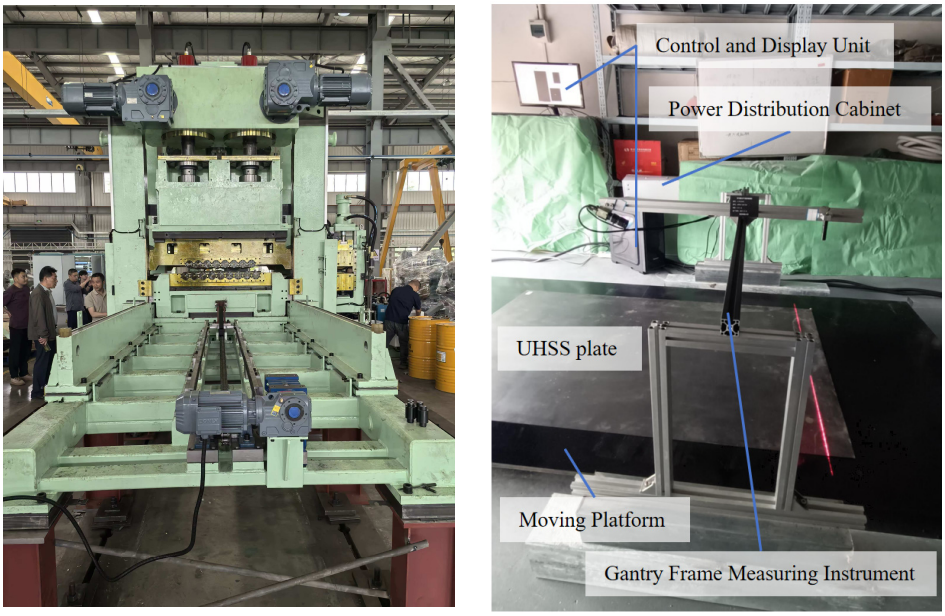
6. Case Study

This paper employs a collaborative optimization approach, taking leveling energy consumption and peak residual stress difference as optimization objectives and post-leveling flatness as a constraint. Due to the limitations of on-site test conditions, it is difficult to measure residual stress accurately and efficiently; therefore, post-leveling flatness and leveling energy consumption are adopted as the core evaluation indicators in experiments. A 17-roll leveler was used to conduct leveling tests on MS1500 ultra-high-strength steel sheets with three typical initial wave heights under original and optimized process parameters. The specific process parameters are shown in Table 12.

Table 12. Domains of Variables.

Scheme No.	Initial Wave Height/mm		Entry Reduction /mm	Exit Reduction /mm	Leveling Speed/m·min^{-1}
1	10.9	Orig.	3.000	2.083	5.800
2		Opt.	2.755	2.215	7.500
3	12.3	Orig.	2.900	2.262	6.500
4		Opt.	2.787	2.202	7.499
5	14.2	Orig.	2.860	2.357	6.900
6		Opt.	2.835	2.197	7.500

Figure 10a shows a schematic diagram of the 17-roll UHSS plate leveling machine. The flatness of the plates before and after leveling was measured using the detection device shown in Figure 10b [31], while energy consumption data was collected directly by the equipment control system.



(**a**) (**b**)

Figure 10. Leveling and measurement of ultra-high-strength steel (UHSS) plates: equipment, measurement system, simulation, and product. (**a**) Multi-roll leveling equipment for UHSS plates; (**b**) Flatness measurement system for plate strips.

As shown in the parameter configurations of the original processes (Schemes 1, 3, and 5) in Table 12, empirical parameter adjustment exhibits obvious randomness: with the increase in wave height, the entry reduction decreases from 3.000 mm to 2.860 mm; however, the changes in exit reduction and leveling speed vary without regular trends. This indicates that the traditional process window relies on manual trial-and-error and empirical judgment, making it difficult to achieve systematic optimization among parameters. In contrast, the optimized processes (Schemes 2, 4, and 6) exhibit a clear parameter-tuning logic: the entry reduction X_2 increases gradually, the exit reduction X_3 shows a decreasing trend, and the leveling speed X_4 approaches the upper limit of 7.5 mm·m^{-1} in all cases. This parameter adjustment pattern indicates that the optimization strategy tends to realize energy consumption control by regulating leveling speed, with the entry reduction dominating the deformation and the exit reduction providing fine-tuning, thereby forming a core control mechanism of "high speed and low reduction." The experimental and simulation results are presented in Table 13 and Figure 11.

Table 13. Comparison of Leveling Simulation and Experiment.

Sample No.	Leveling Energy/KJ		Flatness/mm·m^{-1}	
	Exp.	Sim.	Exp.	Sim.
1	241.76	223.82	−3.27	−3.22830
2	187.58	180.89	−3.39	−3.41416
3	209.46	195.61	−3.66	−3.58364
4	185.40	177.15	−3.44	−3.47834
5	203.95	192.34	−4.26	−4.24651
6	187.45	174.53	−3.43	−3.45347

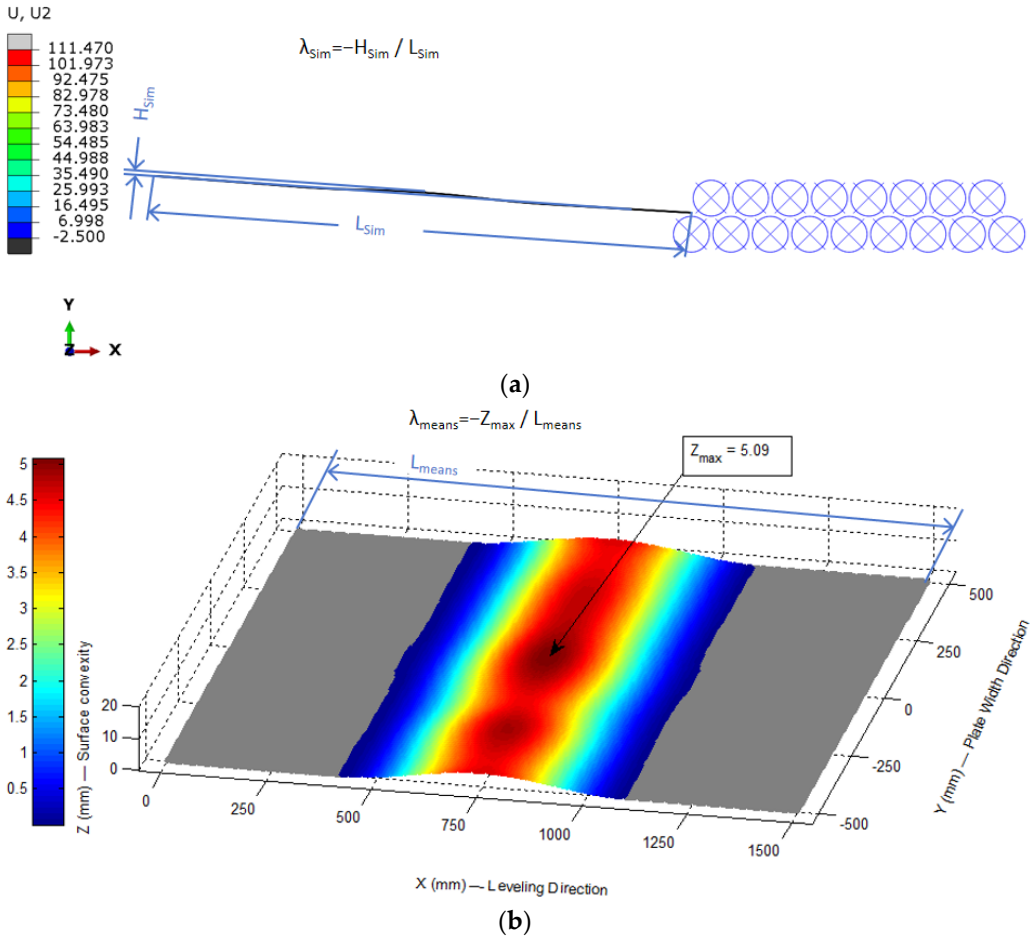


Figure 11. Comparison of post-leveling flatness between simulated and experimental results for Scheme 2. (**a**) Simulated post-leveling flatness result $\lambda_{Sim} = -3.41416$; (**b**) Laser-scanned post-leveling flatness result $\lambda_{means} = -3.390$.

The average relative error for the leveling energy consumption index was 5.77%, the average absolute error was 11.88 kJ, and the maximum relative error was 7.42% (Scheme 1). The simulation–experiment deviation for energy consumption was significantly greater than that for the flatness index. The primary reasons for this phenomenon are as follows: First, the simulation model did not account for the friction energy loss between the roll plates; second, the energy consumption calculation did not account for the no-load power consumption of each roll. The average relative error of the flatness indicators after leveling for the six sets of schemes was 1.03%, the average absolute error was 0.0363 mm·m^{-1}, and the maximum relative error was 2.09% (Scheme 3). The error values for the optimized processes (2, 4, 6) (0.71%, 1.11%, 0.68%) were generally lower than those of the original process samples (1.28%, 2.09%, 0.32%), indicating that the surrogate model's predictive accuracy within the optimized parameter neighborhood was significantly superior to that in the non-optimized regions. The reduction in energy consumption for the optimized processes was significantly greater than the improvement in sheet flatness; this phenomenon reveals that the core contribution of the optimization strategy lies in energy savings rather than further reduction in residual stress. It indicates that within the process range of initial wave heights of 10.5–14.6 mm, the flatness metrics of the original process were already close to the design threshold, and the marginal benefits of further optimization were diminishing, whereas energy consumption optimization still held considerable potential. The optimized process generally increases the leveling speed to the upper limit of 7.5 m·min^{-1}, reduces the entry reduction by 0.2–0.3 mm, and fine-tunes the exit reduction by ±0.05 mm.

This "high-speed, low-reduction" strategy essentially utilizes the strain rate hardening effect (Equation (4)) to maintain the leveling force level while shortening the integration time for energy consumption per unit length, thereby achieving a balance between energy consumption and quality metrics.

The results indicate the constructed surrogate model exhibits high accuracy within the optimized parameter neighborhood (flatness error < 2.1%, energy consumption error < 8.0%), verifying the engineering feasibility of the energy–quality balanced optimization strategy in the leveling process of ultra-high-strength steel. The optimized process achieves a significant reduction in energy consumption while ensuring compliance with flatness standards, providing a technical pathway for overcoming the current bottlenecks in the leveling process of ultra-high-strength steel.

7. Conclusions

An "energy–quality balanced" optimization framework was developed for the multi-roll leveling process of ultra-high-strength steel, and an adaptive process control strategy tailored to the incoming material condition was established. The following conclusions were drawn:

1. Based on the Box–Behnken experimental design and finite element simulation, a multi-response surrogate model was developed based on response surface methodology, with initial wave height, entry/exit reductions, and leveling speed as inputs, and leveling energy consumption, post-leveling flatness, and peak residual stress difference as outputs. The model exhibits a good fit ($R^2 > 0.95$) and achieves high prediction accuracy for leveling energy consumption and post-leveling flatness deviation; for the peak residual stress difference, the model also effectively captures its evolution trends with respect to process parameters. Overall, the developed surrogate model provides an effective analytical tool for elucidating the nonlinear coupling relationships between process parameters and performance objectives during the leveling process of ultra-high-strength steel.
2. An energy–quality co-optimization model oriented toward "low energy consumption and low residual stress difference peak" was established. Using the NSGA-II algorithm and the TOPSIS decision-making method, the Pareto optimal solution set was obtained, and the optimal process parameters were selected. Adaptive recommendation curves for process parameters were established for initial wave heights ranging from 10.5 to 14.6 mm, revealing the control pattern where "the entry reduction increases with wave height, the exit reduction fluctuates within a range, and the leveling speed stabilizes at a high-speed range," thereby forming a "high-speed, low-reduction" control strategy; traditional empirical parameter tuning lacks clear patterns of change and is notably arbitrary. This provides a feasible strategy for the intelligent adaptive control of the leveling process.
3. Case studies indicate that leveling using the optimized process parameters yields high-quality sheets with a post-leveling flatness better than 3.5 $mm \cdot m^{-1}$. The flatness of the original process was already close to the performance threshold, leaving limited room for further optimization, while energy consumption during leveling was significantly reduced. The simulation results agree well with the experimental data, with a maximum relative error of less than 8%, effectively verifying that the finite element model, response surface model, and optimization decision-making framework established in this paper possess high reliability and engineering applicability. It was also confirmed that the model's predictive accuracy is significantly better within the optimized parameter region than in non-optimized regions. The discrepancy between simulation and experimental results for leveling energy consumption primarily

stems from unaccounted factors such as roller-sheet friction, power consumption, and no-load power consumption of the leveling rolls.

The theoretical framework and practical solutions developed in this study not only provide direct guidance for addressing the challenge of energy–quality balance in the leveling process of ultra-high-strength steel but also offer scalable solutions for the intelligent transformation and green emission reduction goals of the high-end sheet metal manufacturing industry.

It should be noted that this paper has the following limitations regarding model validation: due to constraints imposed by on-site testing conditions, no actual measurements were taken to verify the residual stresses after leveling; this work will be carried out by a collaborating institution in future research. Furthermore, the model presented in this paper was developed based on MS1500 steel, a plate thickness of 3 mm, and specific defect types, and does not account for factors such as initial residual stresses and elastic deformation of the roll train. Future research will be extended to different plate thicknesses and grades of ultra-high-strength steel, further covering various plate defect patterns, and will incorporate online data-driven methods to achieve real-time intelligent control of the leveling process.

Author Contributions: Conceptualization, J.C., Y.G. and Z.Z.; methodology, B.F. and Z.Z.; software, B.F.; validation, B.F. and J.C.; formal analysis, X.X.; investigation, L.W.; resources, X.X.; data curation, B.F. and Y.G.; writing—original draft preparation, B.F.; writing—review and editing, Z.Z., X.X. and L.W.; visualization, J.C. and Y.G.; supervision, L.W.; project administration, L.W.; funding acquisition, L.W. All authors have read and agreed to the published version of the manuscript.

Funding: The authors would like to thank the National Natural Science Foundation of China (Grant Nos. 72471181 and 52275503), Outstanding Youth Foundation of Hubei Province (Grant No. 2023AFA092), and Wuhan Natural Science Fund Special Zone Program (Grant No. 2025041001010355).

Data Availability Statement: The original contributions presented in this study are included in the article. Further inquiries can be directed to the corresponding authors.

Conflicts of Interest: The authors declare no conflicts of interest.

Nomenclature

$\kappa_0^{(2)}$	corresponding initial curvature
w_0	initial wave height of the arc-shaped defect
L_0	chord length of the arc-shaped defect
κ_w	reverse curvature
δ	reduction amount of the current roll
t	roll pitch
H	sheet thickness
$\dot{\varepsilon}(z)$	average single-roll plastic strain rate
z	distance from the neutral plane of the cross-section
v_0	critical speed of the material
v	leveling speed
σ_0	the quasi-static yield strength
E	Young's modulus
σ_f	flow stress generated under quasi-static deformation
D	material's strain rate coefficient
p	strain rate exponent
M	leveling bending moment
κ_r	residual curvature

$\sigma_{res}(z)$	residual stress field in the cross-section
P	leveling energy consumption
ω	angular velocity of the working roll
L_t	length of the strip to be leveled
R	radius of the leveling roll
$\kappa_{res}^{(n-1)}$	residual curvature of the n − 1th leveling roll
λ	post-leveling flatness
$\Delta\sigma_{max}$	peak residual stress difference

References

1. Geng, R.M.; Cui, Y.E.; Wu, B.; Li, Y.; Wang, C.X.; Li, Y. Characteristics of microstructures and mechanical properties of 3 GPa ultrahigh strength maraging steel. *J. Aeronaut. Mater.* **2024**, *44*, 151–158.
2. Yang, C.; Ye, B.; Ma, Y.; Zhang, M.D.; An, D.M.; Gao, Q.; Zhou, F. Progress in the Surface Protection Technology of Aerospace Ultra-High Strength Steel. *Mater. Prot.* **2024**, *57*, 87–101.
3. Morris, J.W.; Hardy, S.J.; Thomas, J.T. Some fundamental considerations for the control of residual flatness in tension levelling. *J. Mater. Process. Technol.* **2002**, *120*, 385–396. [CrossRef]
4. Wang, X.G.; Zhu, X.Y.; Han, P.S. Calculation Model of Residual Stress During Quenching and Straightening of High-strength Plate. *Adv. Eng. Sci.* **2021**, *53*, 166–172.
5. Hibino, F. The practical formula for leveling strain in a roller leveler. *J. Jpn. Soc. Technol. Plast.* **1990**, *31*, 208–212.
6. Doege, E.; Menz, R.; Huinink, S. Analysis of the levelling process based upon an analytic forming model. *CIRP Ann.* **2002**, *51*, 191–194. [CrossRef]
7. Wang, Z.G.; Wang, H.; Li, Y.R. Method for calculating the intermesh of straightener and its influence on straightening quality. *J. Wuhan Univ. Sci. Technol.* **2009**, *32*, 347–350.
8. Liu, Z.F. Influence of rolling reduction on key parameters in the straightening process of plate. *Forg. Stamp. Technol.* **2015**, *40*, 109–113.
9. Kuo, S.-K.; Ou, Y.-L.; Wang, D.-A. An Analytical Model for Stress and Curvature Prediction of a Strip Leveling Process. *Metals* **2022**, *12*, 757. [CrossRef]
10. Xue, J.A.; Hu, X.L.; Liu, X.H.; Wang, G.D. Mathematical Model of Elastic-Plastic Bending for Roller Leveling. *J. Iron Steel Res.* **2008**, *20*, 33–36.
11. Yi, G.D.; Gu, Y.; Qiu, L.M.; Wang, C. Multi-roll levelling method for longitudinal waves in metal sheet based on a coupled curvature integration model. *Int. J. Adv. Manuf. Technol.* **2020**, *106*, 2721–2734. [CrossRef]
12. Yi, G.D.; Liang, Y.; Wang, C.; Xu, J.H. Evolution of Residual Stress Based on Curvature Coupling in Multi-Roll Levelling. *Appl. Sci.* **2019**, *9*, 4975. [CrossRef]
13. Morris, J.W.; Hardy, S.J.; Thomas, J.T. Effects of tension levelling process parameters on cold rolled strip characteristics using a designed factorial analysis approach. *Ironmak. Steelmak.* **2013**, *32*, 443–448.
14. Morris, J.W.; Hardy, S.J.; Lees, A.W.; Thomas, J.T. Formation of residual stresses owing to tension levelling of cold rolled strip. *Ironmak. Steelmak.* **2001**, *28*, 44–52. [CrossRef]
15. Gong, B.Y.; Wang, Z.G.; Li, Y.R.; Zhang, H.W.; Huang, J. Finite element analysis for the residual stress of plate during straightening process. *J. Plast. Eng.* **2010**, *17*, 116–120.
16. Sun, L.; Zhao, Z.Y. Effects of Bending on Plate Shape and Residual Stress in Straightening Process by 17-Roll Straightener. *Hot Work. Technol.* **2014**, *43*, 96–99.
17. Grüber, M.; Kümmel, L.; Hirt, G. Control of residual stresses by roller leveling with regard to process stability and one-sided surface removal. *J. Mater. Process. Technol.* **2020**, *280*, 116600. [CrossRef]
18. Grüber, M.; Hirt, G. Investigation of correlation between material properties, process parameters and residual stresses in roller levelling. *Procedia Manuf.* **2018**, *15*, 844–851. [CrossRef]
19. Grüber, M.; Hirt, G. A strategy for the controlled setting of flatness and residual stress distribution in sheet metals via roller levelling. *Procedia Eng.* **2017**, *207*, 1332–1337. [CrossRef]
20. Gribkov, E.P.; Kovalenko, A.K.; Hurkovskaya, S.S. Research and simulation of the sheet leveling machine manufacturing capabilities. *Int. J. Adv. Manuf. Technol.* **2022**, *120*, 743–759. [CrossRef]
21. Ye, G.P.; Wu, K.; Sun, Y.; Zhang, H.W.; Fu, W.A.; Kong, D.W. Numerical simulation and process analysis on eleven-roll leveling process for plastic reinforced materials. *Forg. Stamp. Technol.* **2021**, *46*, 84–91.
22. Wang, H.H.; Wu, B.X.; Higuchi, T.; Yanagimoto, J. Tension Leveling Using Finite Element Analysis with Different Constitutive Relations. *ISIJ Int.* **2020**, *60*, 1273–1283. [CrossRef]

23. Wang, H.H.; Wu, B.X.; Yanagimoto, J. Elastic-Plastic Finite Element Analysis of Tension Leveling with Non-Associated Flow Rule and Mixed Hardening. *Steel Res. Int.* **2019**, *90*, 1800401.
24. Guo, X.P.; Fang, W.X. Influence of straightening speed of heavy rail on residual stress after straightening. *Forg. Stamp. Technol.* **2015**, *40*, 58–61.
25. Wang, J.L.; Zhu, X.Y.; Wang, X.G. Prediction model of plate roller straightening process based on GA-BP neural network. *Mod. Manuf. Eng.* **2023**, *515*, 115–120.
26. Nan, W.J.; Wang, L.X. Process parameters prediction of intelligent straightening system based on Sine-SSA-BP algorithm. *J. Plast. Eng.* **2024**, *31*, 81–89.
27. Hu, Y.; Yuan, J.C.; Lü, C. Research and application of an intelligent optimization process prediction model for roller straightening process. *Mod. Manuf. Eng.* **2024**, *527*, 109–117.
28. Wang, G.Q.; Li, J.D.; Han, B.; Li, Y. Analysis of medium and heavy plate shape in roll straightening based on finite element simulation. *Steel Roll.* **2024**, *41*, 188–194.
29. Cheng, J.J. Research on Springback and Twist of Ultra High Strength Steel Thin-Walled Components with Asymmetric Section in Roll Forming Process. Ph.D. Thesis, University of Science and Technology Beijing, Beijing, China, 2023.
30. Cao, H.L. Properties under high strain rate and characterization model of high strength low alloy steel HC340LAD+Z based on modified Cowper-Symonds model. *Forg. Stamp. Technol.* **2025**, *50*, 286–296.
31. Wang, Y.; Zhao, L.L.; Cui, X.M.; Zhu, X.Q. Simulation analysis of straightening process and design of reduction schedule parameters for nine-roller straightener. *J. Plast. Eng.* **2019**, *26*, 293–300.
32. Yang, X.; Yu, W.; Tang, D.; Fan, J.; Li, Y.Q.; Wang, H.L.; Du, Q.M. Study on Straightening Process of Insufficient Deformation of High Strength Steel Medium Thick Plate. *Hot Work. Technol.* **2021**, *50*, 84–89.
33. Xia, X.X.; Wang, L.; Wang, L.; Zhang, Z.L.; Liu, X. High-efficiency flatness detection method for medium-thick steel plates based on multiline parallel laser vision. *Opt. Eng.* **2023**, *62*, 26. [CrossRef]
34. Lü, G.J.; Ji, T. Mechanical Properties of Ternary Polymer Mortar Based on Response Surface Method. *J. Build. Mater.* **2021**, *24*, 970–976.
35. Wang, H.B.; Cui, T.; Chen, J.; Wang, W.; Tan, K.H.; Yang, D.L.; Zhang, T.S. Mix Proportion Optimization and Performance Study of Manufactured Sand Road Concrete Based on Response Surface Methodology. *Bull. Chin. Ceram. Soc.* **2024**, *43*, 1878–1888.
36. Wang, P.B.; Yin, G.S.; Feng, J.J.; Sun, R.; Liu, Y.H.; Zhu, D.F.; Ma, R.J.; Gao, Z.; Zhang, Y.J. Multi-Objective Optimization of Mix Proportion of Hybrid Fiber Recycled Aggregate Concrete Based on NSGA-II and Entropy Weight TOPSIS Method. *Bull. Chin. Ceram. Soc.* **2022**, *41*, 4189–4201.
37. Wang, Z.W.; Zhang, Z.G.; Cai, W.J.; Zhang, W.; He, Z.; Liu, J.W.; Xin, Z.B.; Wang, Y.N.; Zhu, R.Q.; Wu, Y.Z.; et al. PID parameter tuning method for hydraulic turbine governor based on NSGA-III and TOPSIS. *Sci. Technol. Eng.* **2024**, *24*, 15639–15645.

Disclaimer/Publisher's Note: The statements, opinions and data contained in all publications are solely those of the individual author(s) and contributor(s) and not of MDPI and/or the editor(s). MDPI and/or the editor(s) disclaim responsibility for any injury to people or property resulting from any ideas, methods, instructions or products referred to in the content.